Food Research International 109 (2018) 223–231

Contents lists available at ScienceDirect

Food Research International

journal homepage: www.elsevier.com/locate/foodres

Infrared spectroscopy as an alternative methodology to evaluate the effect of structural features on the physical-chemical properties of inulins

Nelson Romano[a], Cuauhtémoc Araujo-Andrade[b], Javier Lecot[a], Pablo Mobili[a], Andrea Gómez-Zavaglia[a,*]

[a] Center for Research and Development in Food Cryotechnology (CIDCA, CCT-CONICET La Plata), La Plata, RA1900 Buenos Aires, Argentina
[b] ICFO-Institut de Ciències Fotòniques, The Barcelona Institute of Science and Technology, Castelldefels, 08860 Barcelona, Spain

ARTICLE INFO

Keywords:
Inulin
Infrared spectroscopy
Multivariate analysis
Amorphous and crystalline states
Melting temperature X-ray diffraction
Differential scanning calorimetry

ABSTRACT

Two types of inulins of different composition were investigated in the glassy and in the crystalline states, at relative humidities within 11 and 97%. The melting and glass transition temperatures (Tm, Tg), and their crystallinity indexes (CI) were determined by modulated differential-scanning calorimetry (MDSC) and wide-angle X-ray scattering (WAXS), respectively. In parallel assays, Fourier transform-infrared spectroscopy (FTIR) coupled to principal component analysis (PCA) enabled a physical-chemical and structural characterization of samples, explaining 90% of the total variance. Finally, partial least square (PLS) models were defined to determine Tg, Tm, and CI directly from the FTIR spectra, using the MDSC and WAXS results as reference methods. In all cases, the mean of predicted values fitted very well those of the reference methods ($R^2 > 0.961$), thus supporting the use of the PLS models to investigate unknown samples. The robustness of the models underlines the usefulness of FTIR to easily determine physical-chemical parameters, otherwise requiring complex preparation of samples and prolonged times of analysis.

1. Introduction

Inulin is a natural polysaccharide present in the leaves, fruits and/or roots of many plants (Jerusalem artichoke, chicory, garlic, asparagus, salsify, dandelion, onion, leek, banana, wheat, rye, barley) (Kaur & Gupta, 2002). As it belongs to the dietary fiber, its incorporation in the formulation of functional foods is very valuable (Sirbu & Arghire, 2017; Tighe-Neira et al., 2017).

From a chemical viewpoint, inulin belongs to the fructan family of carbohydrates and is composed of fructose units linked by β-(2→1) glycosidic bonds and a terminating D-glucosyl moiety (Romano, Schebor, Mobili, & Gomez-Zavaglia, 2016). The length of the fructose chains ranges from 2 to 60 monomeric units, and inulins containing maximally 10 fructose units are also known as oligofructose (Romano et al., 2016). Commercial inulins are mixtures of oligo and polysaccharides of different degrees of polymerization (DP).

From a physical perspective, inulin can exist in the glassy or in the crystalline phase. The glass transition temperature (Tg) is the range of temperatures at which amorphous materials pass from the amorphous to the rubbery state (Santos, Araujo-Andrade, Tymczyszyn, & Gomez-Zavaglia, 2014). Glass transition occurs at a given temperature which is dependent on the water content and also a key parameter to set-up storage conditions (Romano et al., 2016; Santos et al., 2014). When the storage temperature is above Tg, amorphous solid matrices are more susceptible to caking (tendency to form lumps or masses rather than being smoothly flowable), leading to undesirable effects on storage (Aguilera, del Valle, & Karel, 1995). In this context, the molecular weight of inulins has a strong influence on the stability of the amorphous states. Although inulins of high average DP are generally more stable (Ronkart et al., 2006; Zimeri & Kokini, 2002) their solubility is much lower (Franck, 2002).

Crystalline states of inulin can be obtained by cooling aqueous solutions with concentrations within 10 and 50% w/v (Glibowski, Pikus, Jurek, & Kotowoda, 2014). The crystallinity of inulins is an important physical-chemical parameter because it determines their stability during storage and their technological properties (Ronkart et al., 2009;

Abbreviations: DP, degree of polymerization; Tg, glass transition temperature; CI, crystallinity index; DSC, differential scanning calorimetry; FTIR, Fourier transform infrared spectroscopy; Tm, melting temperature; MDSC, modulated differential scanning calorimetry; PCA, principal component analysis; PLS, partial least square analysis; HP, inulin ≥23 (containing oligosaccharides with DP ≥23); IQ, inulin 3-60 (containing oligosaccharides with DP from 3 to 60); HP-a, amorphous HP inulin; HP-c, crystalline HP inulin; IQ-a, amorphous IQ inulin; IQ-c, crystalline IQ inulin; RH, relative humidity; HPAEC, high performance anion exchange chromatography; A, area under the band at $10° < 2\theta < 15°$; RMSEC, root mean square error of calibration; RMSEP, root mean square error of prediction; ANOVA, analysis of variance; WAXS, wide-angle X-ray scattering

* Corresponding author at: Center for Research and Development in Food Cryotechnology (CIDCA, CCT-CONICET La Plata), Calle 47 y 116 La Plata, Buenos Aires 1900, Argentina.
E-mail address: angoza@qui.uc.pt (A. Gómez-Zavaglia).

https://doi.org/10.1016/j.foodres.2018.04.032
Received 19 February 2018; Received in revised form 13 April 2018; Accepted 15 April 2018
Available online 18 April 2018
0963-9969/

Ronkart, Deroanne, et al., 2010; Ronkart, Paquot, et al., 2010). In this sense, the hydrogen bonds established between hydrated (or hemi-hydrated) crystalline forms of inulins and water molecules act as stabilizing forces (André et al., 1996).

The low dissolution of dehydrated inulins, as well as their hygroscopicity, are clearly undesirable effects when intended to be incorporated in the formulation of functional foods (Aguilera et al., 1995). The solubility of dehydrated inulins is directly related to their DP and their physical state (Bot, Erle, Vreeker, & Agterof, 2004). The higher the DP the lower the solubility (Franck, 2002; Mensink, Frijlink, Voort Maarschalk, & Hinrichs, 2015). Furthermore, at the same temperature, amorphous inulins are less dispersible than crystalline ones (Bot et al., 2004).

Inulin powders are usually analyzed by determining their wide-angle X-ray scattering (WAXS) and their thermal transitions by differential scanning calorimetry (DSC) (Barclay et al., 2016). Although the reliability of such methods is doubtless, they require expensive equipment, determinations are time-consuming and involve specialized operators. Other techniques such as Fourier transform infrared spectroscopy (FTIR), could provide physical and chemical information, including structural aspects, in an easy, quick and reliable way. As bands in the FTIR originate in changes in the dipole moments of the studied compounds, and hydrogen bonds are polar interactions, this technique is particularly useful for studying processes involving the formation and breaking of such intermolecular interactions. In this sense, it must be underlined that the glassy state is characterized by weak hydrogen bonds between the carbohydrates hydroxyl groups. Contrarily, the rubbery state is dominated by stronger hydrogen bonds, established between the carbohydrate hydroxyl groups and water (Wolkers, Oliver, Tablin, & Crowe, 2004). These structural features are useful for their physical characterization and can be determined by FTIR (Santos et al., 2014). The significant disorder of the glassy phases leads to broad spectral bands, typical from this phase. In contrast, the characteristic organization of the crystalline phases originates much narrower bands (Gomez-Zavaglia & Fausto, 2003). Considering that FTIR does not require exogenous chemical reagents, samples need almost no preparation and analytical testing does not generate hazardous waste, this technique appears as an adequate and sensitive approach for the characterization of amorphous and crystalline phases of inulin.

Taking into account that the physical states of inulins (crystalline, glass, rubbery) directly determine their stability during storage, a quick and reliable analysis of these properties would be useful for an adequate selection of inulins, aiming at technological processing. For this reason, a deep investigation of two types of inulins [one of them composed of high DP carbohydrates (HP-inulin), and the other one, of low DP carbohydrates (IQ-inulin)] was carried out in this work. To this aim, amorphous and crystalline inulins were equilibrated at relative humidities (RH) within 11 and 97%. Their melting and glass transition temperatures (Tm, Tg), as well as their crystallinity index (CI), were determined by modulated differential-scanning calorimetry (MDSC) and WAXS, respectively. In parallel, a physical-chemical and structural analysis of all samples was carried out by FTIR. Principal component analysis (PCA) carried out on the FTIR spectra enabled the grouping of samples on the basis of structural and physical aspects. Partial least square (PLS) models were defined to determine Tg, T and CI directly from the FTIR spectra, using the MDSC and WAXS results as references.

2. Materials and methods

2.1. Materials

Inulin 3–60 (IQ inulin) (Frutafit IQ®, Sensus, Roosendaal, The Netherlands), containing oligosaccharides with DP from 3 to 60. Inulin ≥23 (HP inulin) (Raftilose HP, Orafti Beneo, Germany), containing oligosaccharides with DP ≥ 23. LiCl, CH_3CO_2K, $MgCl_2$, K_2CO_3, $Mg(NO_3)_2$, $NaNO_2$, NaCl, KCl, CH_3CO_2Na and K_2SO_4 were obtained from Anedra, (Buenos Aires, Argentina). 1-kestose, nystose and 1^F-fructofuranosylnystose were obtained from Wako Chemicals (Richmond, VA, USA), and sucrose, glucose and fructose, from Sigma Chemical (St. Louis, MO, USA).

2.2. Methods

2.2.1. Composition of IQ and HP inulins

The composition of IQ and HP inulins was determined by high performance anion exchange chromatography (HPAEC), using a Dionex ICS-3000 HPLC system equipped with a pulse amperometric detector (Ronkart et al., 2006). A CarboPac PA-100 ion-exchange analytical column (4 × 250 mm) (Dionex™, Thermo Fisher Scientific, Waltham, MA, USA) equipped with a guard column CarboPac PA-100 (4 × 50 mm) (Dionex™, Thermo Fisher Scientific, Waltham, MA, USA) was eluted with a linear gradient from 0 to 500 mM CH_3CO_2Na in 100 mM NaOH at a flow rate of 0.9 mL/min at 25 °C during 60 min. External standards of fructose, glucose, sucrose, 1-kestose (DP3), nystose (DP4) and 1^F-fructofuranosylnystose (DP5) were used to determine their retention times and check the linear range of the measurements.

2.2.2. Obtaining of amorphous and semi-crystalline inulins

20% w/v suspensions of both IQ and HP inulins were heated at 95 °C under shaking (100 rpm, 15 min) to eliminate the initial crystalline structures and allow a complete dissolution. Scheme 1 shows the experimental protocol.

2.2.2.1. Amorphous inulin samples. The 20% w/v inulin solutions were spray-dried at a pilot scale on an Armfield FT80 spray-dryer (DY, United Kingdom) at a constant air inlet temperature of 160 °C and an outlet temperature of 65 ± 5 °C, to avoid spontaneous crystallization. The resulting powder was named “amorphous inulin” (HP-a and IQ-a), as it appears in the following sections.

2.2.2.2. Semi-crystalline samples. In parallel assays, the 20% w/v solutions of inulin were stored at 4 °C for 72 h under shaking (100 rpm). Crystallization was monitored by registering the absorbance at 700 nm in a UV–vis spectrophotometer (Shimadzu, Kyoto, Japan), according to Cooper et al. (2015). The obtained crystals were centrifuged at 10000 × *g* for 30 min. The supernatants were named “non-crystalline fractions” and were not further used in the present work. The pellets were resuspended in milli Q-water to the original volume and then, spray-dried at a constant air inlet temperature of 160 °C and an outlet temperature of 65 °C. The resulting powder was named “crystalline inulin” (HP-c and IQ-c), as it appears in the following sections, even when in rigor it consists in semi-crystalline samples presenting different degrees of crystallinity.

2.2.3. Equilibration procedure

The amorphous and crystalline spray-dried samples, obtained as explained in Section 2.2.2, were equilibrated for 30 days at 20°C in atmospheres of the following saturated salts: LiCl, CH_3CO_2K, $MgCl_2$, K_2CO_3, $Mg(NO_3)_2$, $NaNO_2$, NaCl, KCl and K_2SO_4, giving relative humidities (RH) of 11, 22, 33, 40, 54, 65, 75, 84 and 97%, respectively (Scheme 1), according to Romano et al., 2016 and Tymczyszyn et al., 2012.

2.2.4. Determining of Tg and Tm

Tg and Tm of amorphous and crystalline samples, equilibrated at RH within 11–97% (Section 2.2.3), were determined by DSC using a Q100 calorimeter (TA Instruments, New Castle, DE, USA), calibrated for the baseline on an empty oven and for temperature and enthalpy with indium (T_{onset}: 156.55 °C; ΔH: 28.82J/g) (Romano et al., 2016). Hermetically sealed 40 μL medium pressure pans containing approximately 5 mg of dehydrated inulins were used (an empty pan served as reference). Thermograms were carried out from −100 °C to 220 °C, at

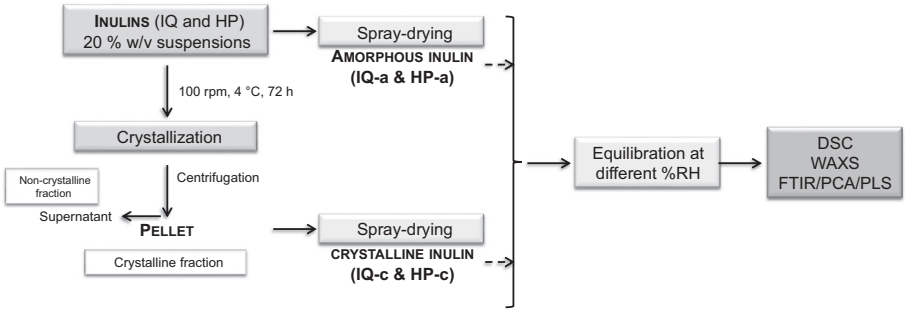

Scheme 1. Experimental protocol for obtaining amorphous and crystalline inulin.

10 °C/min heating rates. The amplitude and period of the MDSC were 0.5 °C/min and 40 s, respectively. The maximum melting temperature and enthalpy were reported for melting processes (Tm), and the middle temperatures, for vitrification processes (Tg).

2.2.5. WAXS

A Xeuss 1.0 laboratory beamline (Xenocs, Sassenage, France) with a Dectris 100 K Pilatus detector and Cu K-α radiation RX source (λ = 1.54178 Å) was used to determine the WAXS. The patterns were recorded at 20 °C using a fixed sample-detector distance (97.49 mm) in the 4° < 2θ < 30° range. Amorphous and crystalline samples equilibrated at RH ranging from 11 to 84% were used for the analyses.

The CI of crystalline samples equilibrated at different %RHs was quantified according to the procedure described in Blundell and Osborn (1983). Briefly, a straight baseline in the 4° < 2θ < 30° range was drawn and subtracted. Then, a scaled amorphous curve was fitted under the diffraction peaks. The ratio of the sum of the areas of the crystalline peaks to the total area was considered to be the CI of the sample.

2.2.6. FTIR

The amorphous and crystalline samples equilibrated at RH within 11–97% (Section 2.2.3) were used to register the FTIR spectra. Approximately 5 mg of each sample was placed on the sample holder of an ATR-FTIR Thermo Nicolet iS10 spectrometer (Thermo Scientific, MA, USA). Spectra were registered in the 4000–500 cm^{-1} range by co-adding 100 scans with 4 cm^{-1} spectral resolution, using OMNIC software (version 8.3, Thermo Scientific, MA, USA). At least 7 spectra were recorded for each sample.

2.2.7. Data analysis

Multivariate analysis and data pre-processing as mean centering and extended multiplicative scatter correction were performed on the FTIR spectra, using The Unscrambler® software (version 9.8, CAMO, Norway).

In order to evaluate the spectral differences among samples arising from amorphous and crystalline states equilibrated at different RHs, PCA was performed on the FTIR spectra, covering the whole range of RH investigated. Taking into account the spectral differences in the PCA scores plot, PLS models were calibrated to determine the CI, Tm, Tg and the area under the band at 10° < 2θ < 15° (A) of both IQ and HP inulins in the amorphous and crystalline states (Esbensen, 2005). FTIR spectra covering the whole range of values, including those obtained from independent experiments and repetitions, were used to define the models. The information regarding the set-up of the PLS models is shown in Table S1. Tg, Tm, CI and A values obtained by MDSC and WAXS were used as reference values. The reliability and robustness of the calibrated models were determined as a function of their correlation values, R-square, BIAS and their calibration and prediction errors (RMSEC and RMSEP, indicating the average difference between predicted and experimentally obtained results). High correlation values and low errors indicate a good capacity to correctly predict or classify unknown samples. The validation of the models was carried out with independently collected spectra (Table S1).

2.2.8. Reproducibility of results

All experiments were performed on duplicate samples using three independent preparations. The relative differences were reproducible irrespective of the preparation employed. Analysis of variance (ANOVA) was carried out using the Infostat v2009 statistical software (Córdoba, Argentina). Differences were tested with paired sample *t*-tests, and if $p < 0.05$ the difference was considered statistically significant.

3. Results and discussion

The composition of IQ and HP inulins is shown in Fig. 1, and the corresponding chromatograms, in Fig. S1. IQ inulin was majorly composed of fructans with DP within 3 and 30. In addition, mono and disaccharides (glucose, fructose, sucrose) represented 13% w/w. On the contrary, HP inulins were mainly composed of fructans with DP within 11–40, all of them occurring in percentages > 10% w/w. Mono and disaccharides were below 2% w/w. The presence of mono and disaccharides in mixtures of fructans strongly determines their technological and functional applications (Romano et al., 2016). For example, inulins of high molecular weight are used as food texture modifiers and fat replacers because of their viscous behavior and their capacity to form gels (Wada, Sugatani, Terada, Ohguchi, & Miwa, 2005). These applications emphasize the importance of determining physical and structural aspects of inulins in a simple manner.

Taking into account both the types of inulins and the treatments to which they were subjected, four kinds of samples were obtained: amorphous IQ and HP inulins (IQ-a and HP-a, respectively), and crystalline IQ and HP inulins (IQ-c and HP-c, respectively) (Scheme 1).

3.1. Physical properties of equilibrated samples

Fig. S2 shows the thermograms of the four types of inulins, determined immediately after spray-drying. Glassy states showed the typical second order transitions. The Tg of HP-a (88.42 ± 2.27 °C) was significantly higher than that of IQ-a (82.12 ± 4.30 °C) ($p < 0.05$), which can be explained considering the presence of fructans of higher DP (Fig. 1B) (Cooper, Barclay, Ginic-Markovic, Gerson, & Petrovsky, 2014; Romano et al., 2016). In addition, weak endothermic peaks were observed above 175 °C for both samples. This indicates the melting of the crystals formed during the processing of samples [ΔH (J/g): 5.79 ± 0.87 (IQ-a); 19.45 ± 0.27 (HP-a)]. On the other hand, no vitreous transitions were observed for IQ-c and HP-c, thus confirming their crystalline character. At higher temperatures, first order endothermic transitions were observed, indicating the melting of crystals. For both IQ-c and HP-c, two endothermic peaks were observed. The first one occurred at Tm = 136 and 121 °C for IQ-c and HP-c, respectively, and the second one, at higher Tm (158 and 167 °C for IQ-c and HP-c, respectively), indicating the presence of two crystals forms. Considering the melting enthalpies of each peak separately, it can be concluded that

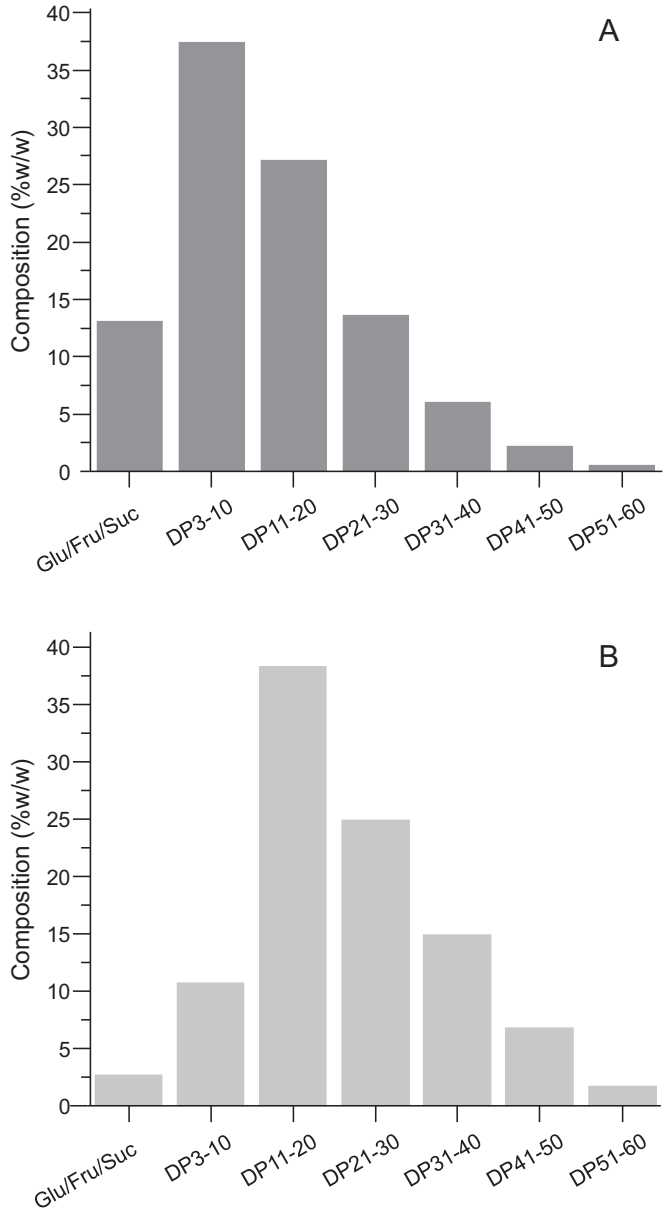

Fig. 1. Carbohydrate composition of inulins. Glu: glucose; Fru: fructose; Suc: sucrose. A. IQ inulin. B. HP inulin.

the HP-c had a higher proportion of low Tm crystals, whereas in IQ-c the contributions of both crystal forms were similar. Furthermore, the total fusion enthalpies indicated the greater crystallization capacity of HP-c [ΔH (J/g): 229.2 ± 3.51 (HP-c); 136.37 ± 5.05 (IQ-c)], which can be explained considering the composition of IQ and HP inulins (Fig. 1). In this regard, it was reported that whereas fructans with DP > 15 facilitate crystallization, the presence of high concentrations of fructans with DP < 15 has an opposite effect (Ronkart et al., 2010).

Fig. 2 shows the Tg of both HP-a and IQ-a inulins equilibrated at different RH. As water is a plasticizer, the higher the RH, the lower the Tg for both inulins. The lower Tg values of IQ-a can be explained considering the presence of lower DP carbohydrates (Fig. 1A). The Tg values are determined by the degree of freedom of the molecules in the amorphous state, which in turn, is directly related to the molecular weight and the polydispersity (molecular weight distribution) (Ronkart et al., 2006). When T-Tg [T: temperature of equilibration (20 °C)] decreases, as a consequence of the increase of RH, amorphous inulins are more susceptible to caking and further crystallization (Aguilera et al., 1995). The kinetics of such undesirable processes are determined by the amount of available water and by the polydispersity of samples (Ronkart, Paquot, et al., 2010).

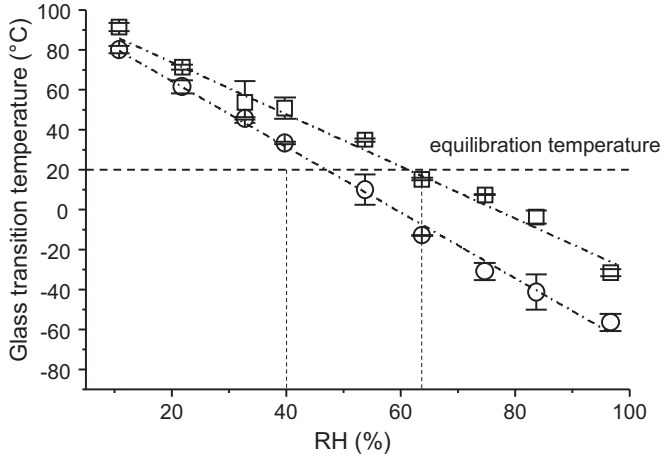

Fig. 2. Glass transition temperature (Tg) of IQ-a and HP-a inulins. Samples were equilibrated at 20 °C, at 11, 22, 33, 40, 54, 65, 75, 84 and 97%RH. Circles: IQ-a; Squares: HP-a. The dashed line at 20 °C indicates the equilibration temperature.

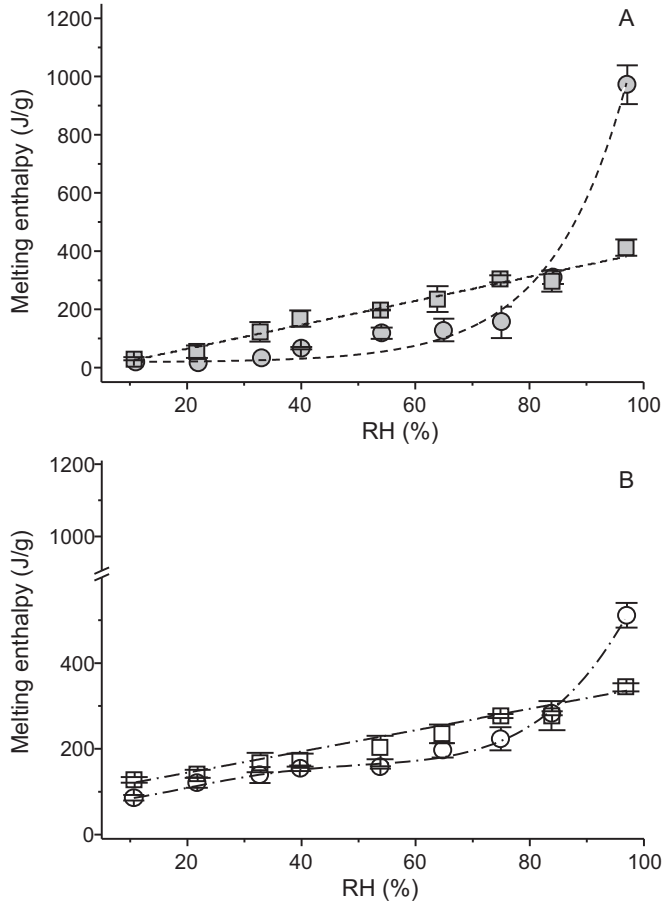

Fig. 3. Melting enthalpy of IQ and HP inulins, as determined by MDSC. Samples were equilibrated at 20 °C, at 11, 22, 33, 40, 54, 65, 75, 84 and 97%RH. A. IQ-a (full circles) and HP-a (full squares). B. IQ-c (empty circles) and HP-c (empty squares).

Fig. 3A depicts the melting enthalpies for IQ-a and HP-a equilibrated at different RH. For both amorphous inulins, the higher the RH

the higher the melting enthalpy, which can be explained considering that inulins are known to crystallize readily from aqueous solution but not from anhydrous media (André et al., 1996). In addition, it is remarkable that, contrarily to HP-a, IQ-a showed no linear response. In particular, almost no increase in the melting enthalpy of IQ-a was observed up to 40%RH (Fig. 3A), which was the highest RH at which such samples remained in the amorphous state at 20 °C (T < Tg, Fig. 2). The melting enthalpy for IQ-a slowly increased from 40 to 84%RH, and a huge increase was observed at 97%RH (Fig. 3A). This delay in the crystallization of IQ-a at low RHs could be ascribed to the presence of low molecular weight fructans (Fig. 1A), which probably preclude the interaction of larger inulin chains with water to form crystals, when the molecular mobility increases (Barclay et al., 2016; Ottenhof, McNaughtan, & Farhat, 2003). On the contrary, a linear increase in the melting enthalpy was observed for HP-a, majorly composed of high molecular weight fructans (Fig. 1B). It can be concluded that crystallization of amorphous inulins (IQ-a and HP-a) was dependent both on the increase in molecular mobility associated to the plasticizing effect of water at high RHs, and on their composition, as low molecular weight fructans delayed crystallization at low RHs.

Fig. 4 shows the appearance of all samples, after equilibration at different RHs at 20 °C. Samples in the amorphous states were lumpy and much less flowable than the crystalline ones. Amorphous samples (IQ-a, HP-a) showed a more agglomerated appearance at RHs < 40%. Note that this observation of lumpiness and lower flowability was more evident for IQ-a inulin, which was that with greater percentages of lower DP carbohydrates (Fig. 1A) and lower Tg (Fig. 2). Typical pictures of collapsed samples were observed at RHs > 54% for IQ-a, and RHs > 65% for HP-a, which is consistent with the corresponding Tgs (Fig. 2). In other words, at 20 °C IQ-a was in the rubbery state at RH > 54% (Tg = 10.12 ± 2.05 °C), and HP-a, at RHs > 65% (Tg = 15.41 ± 0.53 °C), this latter forming smaller agglomerates (Fig. 4). In such conditions of RH, the temperature of equilibration (20 °C) was greater than Tg, thus samples were in the rubbery state (Figs. 2, 4). It is important to underline that the great adsorption of water in the rubbery states increased the volume of the collapsed samples (Fig. 4).

Fig. 3B shows the melting enthalpies of IQ-c and HP-c at different RHs. Both IQ-c and HP-c showed an increase in the melting enthalpy with the increase of RH. This increase of crystallinity was linearly dependent on the RH for HP-c (Melting enthalpy = 247.7 × RH + 95.4 J/g). On the contrary, the melting enthalpy of IQ-c did not significantly change below 40% RH. Above such RH, a non-linear increase was observed, with a maximum at 97%RH (510.55 ± 28.77 J/g). When compared with the counterparts IQ-a and HP-a, both IQ-c and HP-c showed a more flowable appearance at all the RHs, with almost none agglomerates or lumps (Fig. 4). They did not show collapse even at high RHs (54–75%RH).

3.2. WAXS

The WAXS patterns of HP and IQ inulins equilibrated at 20 °C at different RHs, are shown in Fig. 5, and the corresponding CI, in Table S2. Diffractograms in the 5° < 2θ < 30° range presented a single and very broadband for the amorphous samples (Fig. 5A, B, dashed lines). On the contrary, crystalline samples showed narrow diffraction bands (solid lines). IQ-a diffractograms were characteristic from the amorphous state up to 40%RH (Fig. 5A), whereas HP-a ones, up to 65%RH (Fig. 5B). This information was consistent with results obtained for Tg (Fig. 2). At RH < 40% the Tgs of IQ-a were below the temperature of analysis (20 °C). In turn, this situation occurred at RH < 54% for HP-a samples. In addition, the Tg of such samples was slightly below 20 °C (15.41 ± 0.53 °C) at 65%RH. Consistently, the diffractogram of HP-a at 65%RH resembled that from an amorphous sample, but with a weak band at 12.3°, indicating the beginning of crystallization (Fig. 5B). It is interesting to note the presence of a weak band at 2θ = 10.45° for IQ-a (Fig. 5A), typical from semi-hydrated amorphous states (André et al., 1996; Ronkart et al., 2009), which decreases when crystallization is completed, that is, when RH increases (Table S2). Such band was not observed in HP-a samples, thus indicating that only IQ-a samples could be obtained in a semi-hydrated state.

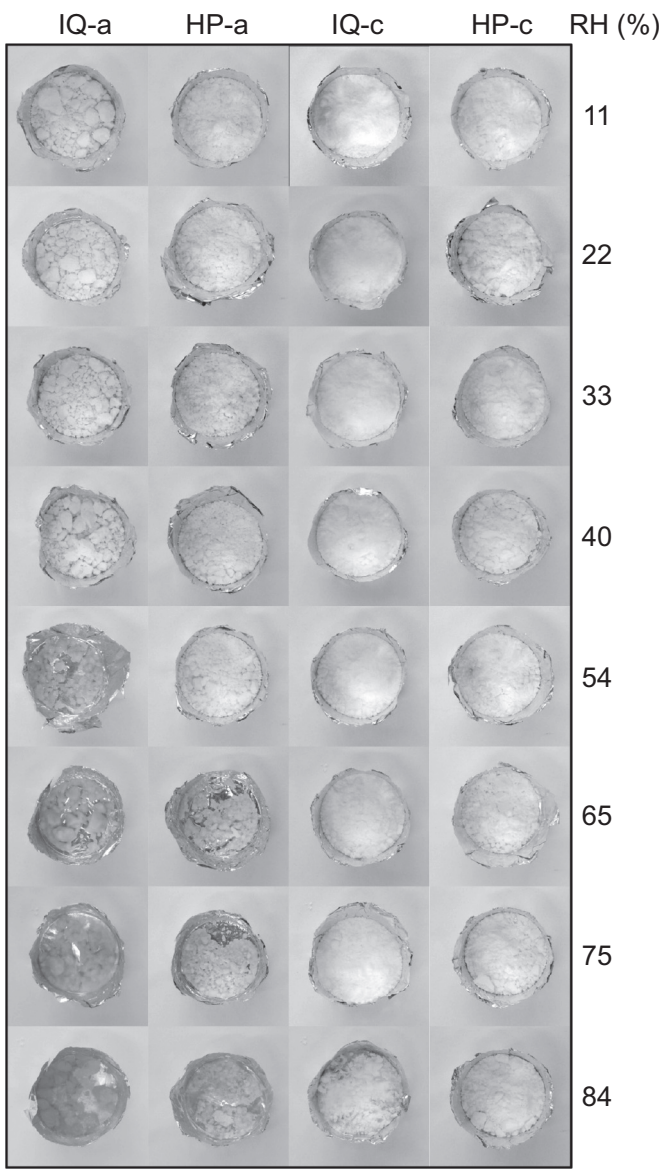

Fig. 4. Photographs of dehydrated IQ and HP inulins, after equilibration for 30 days at T = 20 °C, at RHs within 11 and 84%. T > Tg at RH above 54 and 65% for IQ-a and HP-a, respectively.

In turn, IQ-c and HP-c diffractograms were typical from highly crystalline samples at all the RHs, although an increase in intensity and sharpness of bands was observed with the increase of RHs (Fig. 5C,D, Table S2). It is interesting to note the presence of a weak band at 2θ = 10.60° for HP-c at 11 and 54%RH (Fig. 5D). This band is typical from semi-hydrated amorphous states and decreases when crystallization is completed, that is, when RH increases. Such band was not observed for IQ-c, a feature reported as typical for monohydrated states (André et al., 1996; Ronkart et al., 2009). Taking into account that monohydrated allomorph inulin converts into the semi-hydrated form during dehydration processes (i.e.: vacuum dehydration) (André et al., 1996), it could be inferred that the HP-c (mostly allomorph monohydrated) would have greater stability during dehydration. On the contrary, HP-c crystals were less stable, consistently with their Tm (Fig. S2). In fact, HP-c had greater melting enthalpies at low temperatures,

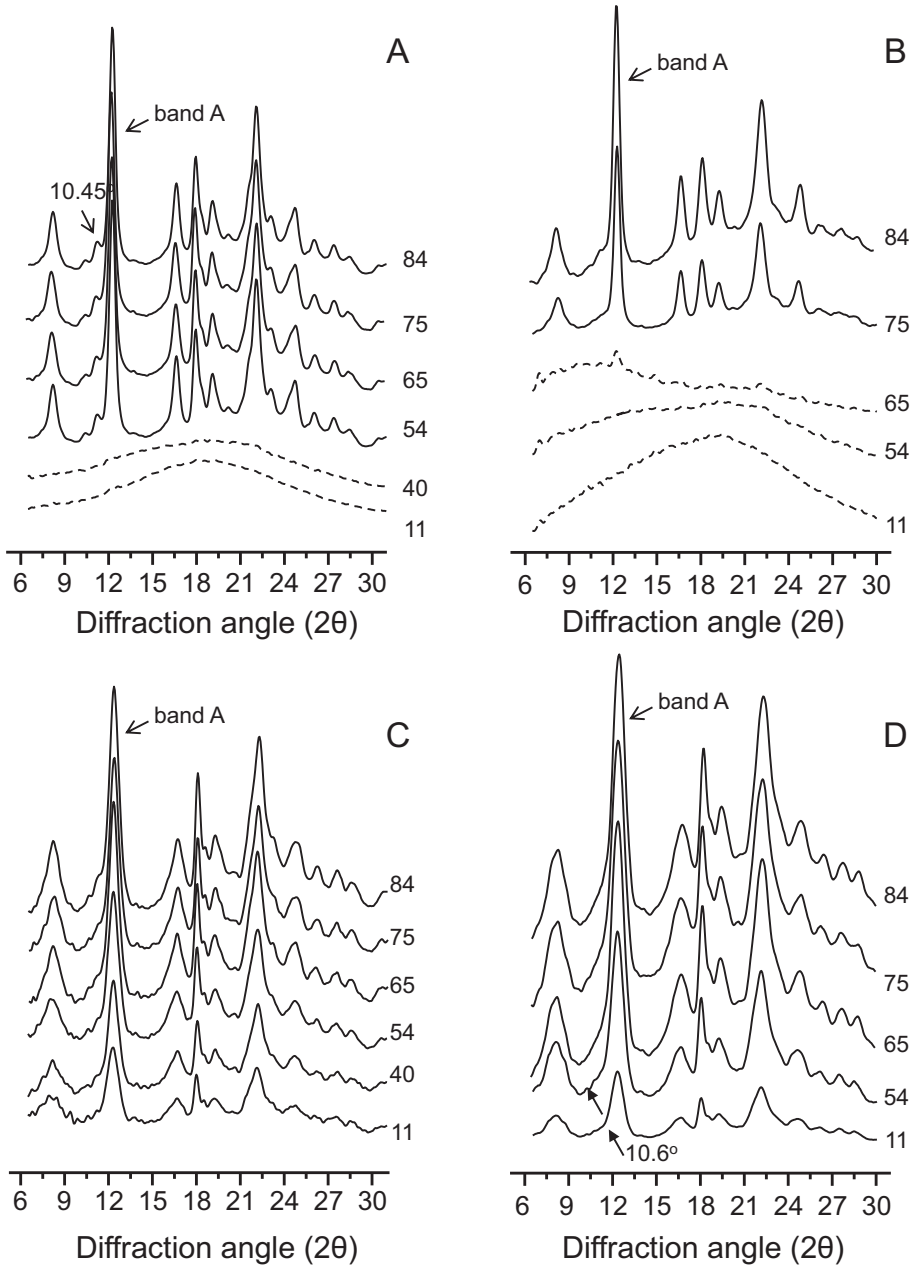

Fig. 5. Diffractograms in the 5° < 2θ < 30° range for inulins equilibrated at different %RH within 11 and 84%. A. IQ-a. B. HP-a. C. IQ-c. D. HP-c. Dashed line diffractograms correspond to amorphous samples.

probably associated to the greater proportion of monohydrated allomorph state.

As water can be almost exclusively adsorbed on the amorphous regions of carbohydrates (Airaksinen et al., 2005), and its uptake can be dependent on the CI of the powders (Mihranyan, Llagostera, Karmhag, Strømme, & Ek, 2004), a deep knowledge of the crystalline structures of carbohydrates has a significant effect on the stability of food and pharmaceutical formulations. In this context, the information obtained in this section represents an important background to define technological applications.

3.3. FTIR

The FTIR spectra of IQ and HP inulins in the amorphous (IQ-a and HP-a) and in the crystalline (IQ-c and HP-c) states, at different RHs are shown in Figs. 6. In the amorphous phase, that is, when T < Tg (RH < 40% and < 54% for IQ-a and HP-a, respectively) (Fig. 2), the spectra were composed of broad bands (Fig. 6A, B). As molecules in the amorphous phase are free to rotate, this disordered state is characterized by broad bands (Gomez-Zavaglia & Fausto, 2003). When T > Tg, that is, for RH > 54% and 64% for IQ-a and HP-a, respectively (Fig. 2), the presence of water molecules and the high molecular mobility of fructans promoted the partial crystallization of the samples. This rearrangement of molecules toward an organized three-dimensional structure that does not freely rotate, resulted in narrower bands, typical from the crystalline state (Gomez-Zavaglia & Fausto, 2003).

The band at 1643 cm^{-1} arose from water molecules embedded either in the amorphous sugar matrix or linked to the crystalline inulins (Santos et al., 2014). After determining the area of that band in the normalized spectra of IQ-a, HP-a, IQ-c and HP-c, the first two samples (IQ-a and HP-a) were those with greater amounts of embedded water (Fig. S3), which is consistent with the higher hygroscopic character of

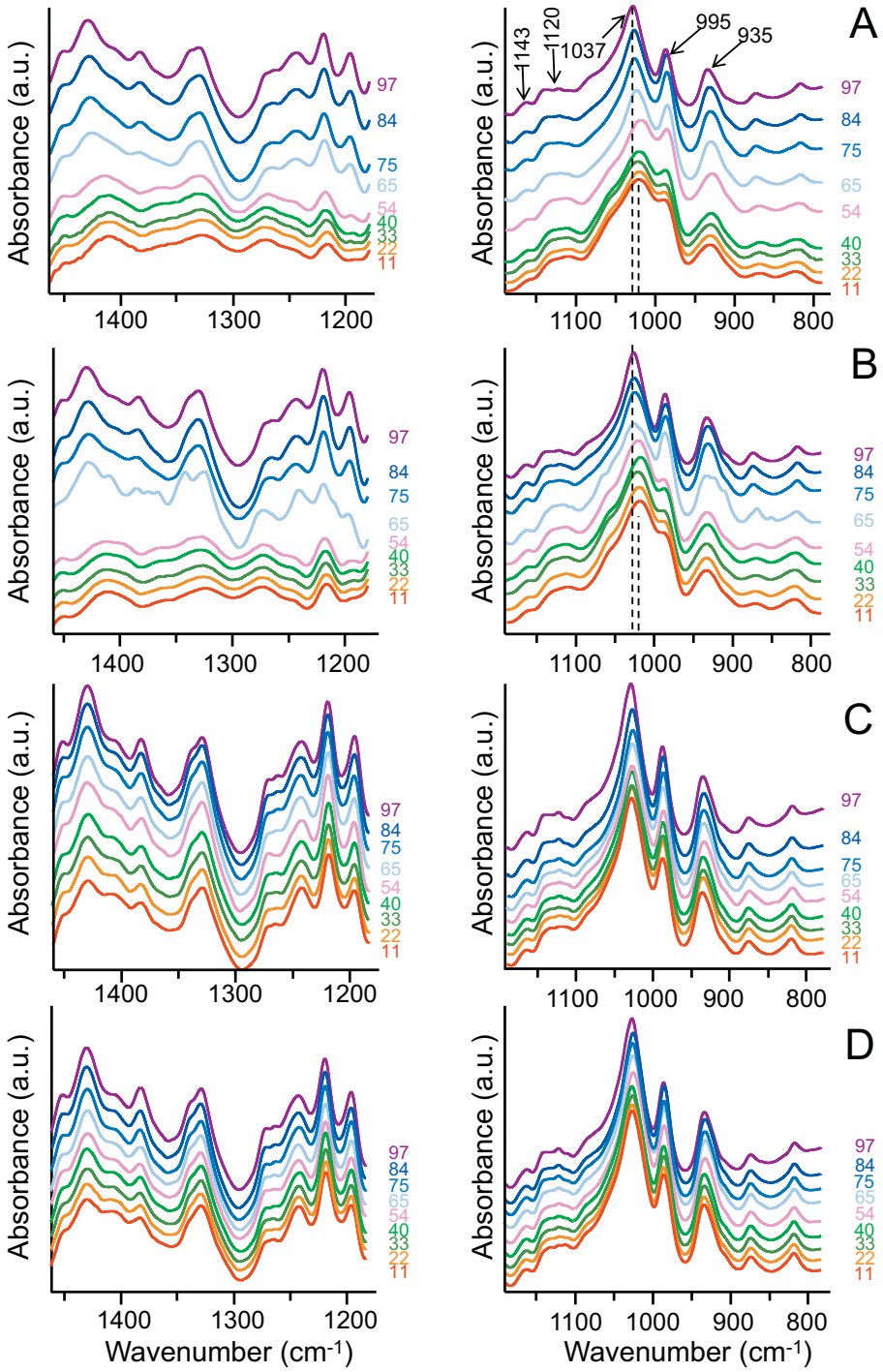

Fig. 6. FTIR spectra of IQ and HP inulins in the 1450–1200 and 1150–800 cm^{-1} regions (left and right side spectra, respectively). Samples were equilibrated at 20 °C, at 11, 22, 33, 40, 54, 65, 75, 84 and 97%RH. A. IQ-a at RH. B. HP-a at RH. C. IQ-c at RH. D. HP-c at RH. Dashed lines in A and B indicate the main shifts resulting from crystallization.

amorphous samples. In addition, IQ inulins had stronger water bands, because of the presence of fructans with lower DP, in agreement with the previous results (Figs. 1-5).

The 1450–1200 cm^{-1} and the 1200–900 cm^{-1} regions were those showing the greatest differences between amorphous and crystalline samples (Fig. 6). The former region arises from the δCH vibrational modes, and the latter, also known as fingerprint region, is a complex region rich in bands ascribed essentially to the C-O-C glycosidic linkage, the δCOH and the νC-C vibrational modes (Santos et al., 2014). In particular, the band at 935 cm^{-1} has been reported as typical from inulin, and ascribed to the β2 → 1 glycosidic bond (Barclay et al., 2016). The increase in the intensity of such band, together with that of bands at 1143, 1120, 1037 and 995 cm^{-1}, is considered as indicative of molecular organization (Barclay et al., 2016). Besides that, the band at 1037 cm^{-1}, ascribed to δCOH vibrational mode, shifted to higher wavenumbers as soon as the RH increased (Fig. 6A,B). This shift, together with the shift of the band at 1643 cm^{-1} to lower wavenumbers (not shown) is the result from the different character of hydrogen-bonds, which are stronger in the crystalline states (Santos et al., 2014).

The FTIR spectra of IQ-c and HP-c were similar to those obtained for

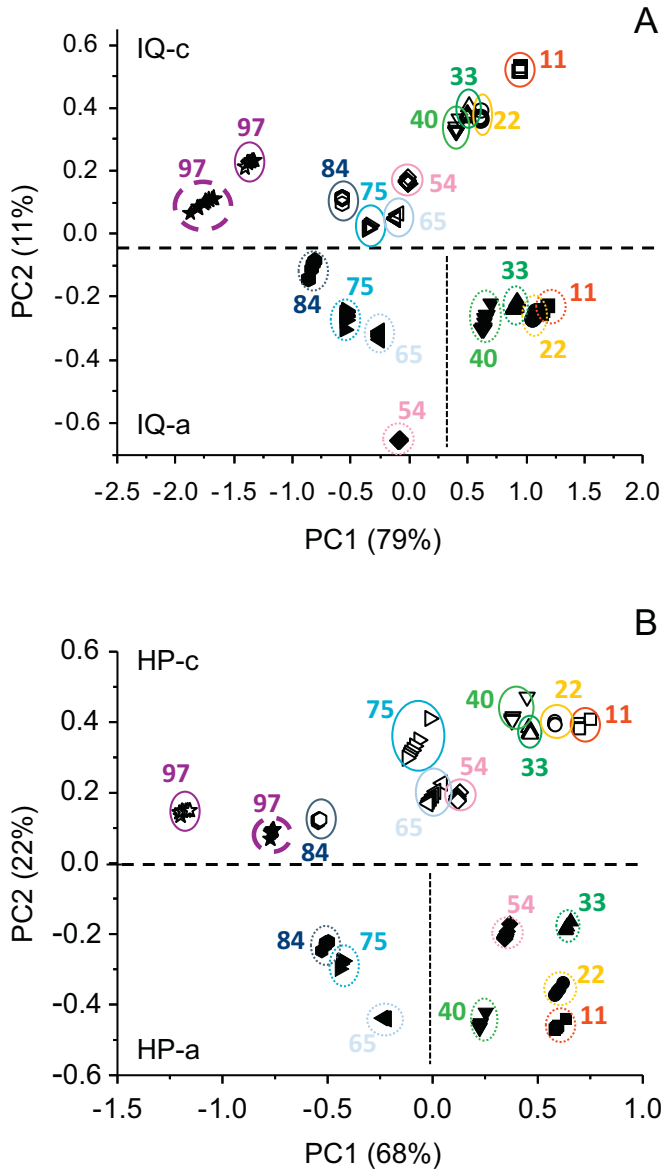

Fig. 7. PCA performed on the FTIR spectra of the amorphous and crystalline inulins, equilibrated at different RHs. A. IQ inulin. B. HP inulin. Full symbols correspond to IQ-a and HP-a, and empty symbols, to IQ-c and HP-c. Squares: 11%RH; circles: 22%RH; up triangles: 33%RH; down triangles: 40%RH; diamonds: 54%RH; left triangles: 65%RH; right triangles: 75%RH; hexagons: 84% RH and stars: 97%RH. To facilitate the visualization, each group was delimited inside colored circles. Full stars groups were denoted inside dash and thick violet circles. Horizontal dashed lines separate IQ-a and HP-a from IQ-c and HP-c, respectively. Vertical dashed lines separate amorphous samples below and above Tg at 20 °C.

the crystallized IQ-a and HP-a (when $T_{equilibration}$ > Tg). The narrow and well defined bands increased their intensity as soon as the RH increased, thus denoting that the higher the RH, the higher the degree of crystallization (Fig. 6C, D), in agreement with the CI obtained by WAXS (Table S2).

3.4. Multivariate analysis

Considering that FTIR spectra showed not only structural but also physical differences among samples, PCA was performed for IQ and HP inulins in the whole range of RHs (Fig. 7). For both inulins, PCA enabled a clear grouping of samples, explaining 90% of the whole variance. According to the loading plots (Fig. S4), the main differences along PC1 arose not only from the fingerprint region (1200–900 cm^{-1}) but also from the 3700–3000 cm^{-1} and 1643 cm^{-1} regions, directly related with the water content. Therefore, the groups observed along PC1 (explaining 79 and 68% of the variance) were clearly related with the RH of samples. Samples equilibrated at the lowest RH were observed at higher PC1 values, and the higher the RH the lower the PC1 values (Fig. 7A, B). Additionally, for IQ-a and HP-a inulins a clear separation between samples above and below the Tg was observed (vertical dashed lines, Fig. 7A, B).

The main differences in PC2 arose from the 1200–900 cm^{-1} region (Fig. S4), and explained 11 and 22% of the variance for IQ and HP inulins, respectively. This PC clearly described the physical character of samples (amorphous and crystalline). Interestingly, both IQ-a and HP-a equilibrated at 97%RH grouped with the crystalline samples (Fig. 5A, B). This can be explained considering that above Tg, the CI of IQ-a and HP-a increased with the RH, attaining values comparable to those of IQ-c and HP-c samples at 97%RH (Table S2).

Finally, different PLS models were defined to determine Tg, Tm, CI and A (area under the band at $10° < 2\theta < 15°$ of the diffractograms) directly from the FTIR spectra, using the MDSC and WAXS results as references. The models were calibrated using between 18 and 27 spectra (Table S1). In all cases, correlation values within 0.936 and 0.999, with R-square above 0.961, were obtained (Table S3). The models were validated with independent sets of data, composed of 15 or 21 spectra collected in the same conditions as those used for calibration (Table S1). Fig. S5 depicts the independent validation results for all the prediction models developed to determine Tg, Tm, CI and A. The root mean square error of prediction (RMSEP) is depicted in the Y-error bars. Using spectra corresponding to all samples (amorphous and crystallines), covering a wide range of values for the parameters analyzed, strengthened the predictive capacity of the models. In all cases, the mean of predicted values fitted nicely the values obtained using the reference methods (Table S3, Fig. S5), thus supporting the use of the PLS models based on FTIR spectra to investigate unknown samples. The capacity of the defined models to predict not only structural but also physical changes underlines their usefulness, converting FTIR in a unique technique, able to determine in a simple way, different parameters of inulins.

4. Conclusions

Considering the huge number of inulin applications in the food and pharmaceutical industries, and the difficulty of amorphous states to be dispersed, a deep knowledge of the structural and physical properties of inulins acquires special importance. Besides the deep analysis of IQ and HP inulins at different RHs, the main achievement of this work was to define PLS models enabling the quick and reliable quantification of physical-chemical parameters of inulins, directly from their FTIR spectra, otherwise requiring complex preparation of samples and prolonged times of analysis.

Supplementary data to this article can be found online at https://doi.org/10.1016/j.foodres.2018.04.032.

Acknowledgments

This project has received funding from the European Union's Horizon 2020 research and innovation program under grant agreement N° 777657, and from the Argentinean Agency for the Scientific and Technological Promotion (ANPCyT) (Projects PICT(2014)/0912; PICT start-up (2016)/4808). Lic. Claudio Reyes and Lib. Diana Velasco are acknowledged for technical assistance. P.M. and A.G.-Z. are members of the research career CONICET. N.R. is postdoctoral fellow from CONICET.

Competing interests

The authors declare that they have no competing interests.

Author's contributions

N.R conceived the work; N.R. and P.M. did the experimental work. C.A. did the multivariate analysis. A.G.-Z coordinated the work (analysis of results, discussion and writing of the manuscript). All authors have approved the final version of the manuscript.

References

Aguilera, J., del Valle, J., & Karel, M. (1995). Caking phenomena in amorphous food powders. *Trends in Food Science & Technology, 6*, 149–155.

Airaksinen, S., Karjalainen, M., Shevchenko, A., Westermarck, S., Leppänen, E., Rantanen, J., & Yliruusi, J. (2005). Role of water in the physical stability of solid dosage formulations. *Journal of Pharmaceutical Sciences, 94*, 2147–2165.

André, I., Mazeau, K., Tvaroska, I., Putaux, J. L., Winter, W. T., Taravel, F. R., & Chanzy, H. (1996). Molecular and crystal structures of inulin from electron diffraction data. *Macromolecules, 29*, 4626–4635.

Barclay, G., Rajapaksha, H., Thilagam, A., Qian, G., Ginic-Markovic, M., Cooper, P. D., ... Petrovsky, N. (2016). Physical characterization and in silico modeling of inulin polymerconformation during vaccine adjuvant particle formation. *Carbohydrate Polymers, 143*, 108–115.

Blundell, D. J., & Osborn, B. N. (1983). The morphology of poly (aryl-ether-ether-ketone). *Polymer, 24*, 953–958.

Bot, A., Erle, U., Vreeker, R., & Agterof, W. G. (2004). Influence of crystallisation conditions on the large deformation rheology of inulin gels. *Food Hydrocolloids, 18*, 547–556.

Cooper, P. D., Barclay, T. G., Ginic-Markovic, M., Gerson, A. R., & Petrovsky, N. (2014). Inulin isoforms differ by repeated additions of one crystal unit cell. *Carbohydrate Polymers, 103*, 392–397.

Cooper, P. D., Harinda Rajapaksha, K., Barclay, T. G., Ginic-Markovic, M., Gerson, A. R., & Petrovsky, N. (2015). Inulin crystal initiation via a glucose-fructose cross-link of adjacent polymer chains: Atomic force microscopy and static molecular modelling. *Carbohydrate Polymers, 117*, 964–972.

Esbensen, K. H. (2005). *Multivariate data analysis-in practice* (5th ed.). Esbjerg, Denmark: CAMO Process AS.

Franck, A. (2002). Technological functionality of inulin and oligofructose. *British Journal of Nutrition, 87*, S287–S291.

Glibowski, P., Pikus, S., Jurek, J., & Kotowoda, M. (2014). Factors affecting inulin crystallization after its complete dissolution. *Carbohydrate Polymers, 110*, 107–112.

Gomez-Zavaglia, A., & Fausto, R. (2003). Low temperature solid-state FTIR study of glycine, sarcosine and N,N-dimethylglycine: Observation of neutral forms of simple α-aminoacids in the solid state. *Physical Chemistry Chemical Physics, 5*, 3154–3161.

Kaur, N., & Gupta, A. (2002). Applications of inulin and oligofructose in health and nutrition. *Journal of Biosciences, 27*, 703–714.

Mensink, M. A., Frijlink, H. W., van der Voort Maarschalk, K., & Hinrichs, W. L. J. (2015). Inulin, a flexible oligosaccharide I: Review of its physicochemical characteristics. *Carbohydrate Polymers, 130*, 405–419.

Mihranyan, A., Llagostera, A. P., Karmhag, R., Strømme, M., & Ek, R. (2004). Moisture sorption by cellulose powders of varying crystallinity. *International Journal of Pharmaceutics, 269*, 433–442.

Ottenhof, M.-A., McNaughtan, W., & Farhat, I. A. (2003). FTIR study of state and phase transitions of low moisture sucrose and lactose. *Carbohydrate Research, 338*, 2195–2202.

Romano, N., Schebor, C., Mobili, P., & Gomez-Zavaglia, A. (2016). Role of mono- and oligosaccharides from FOS as stabilizing agents during freeze-drying and storage of Lactobacillus delbrueckii subsp. bulgaricus. *Food Research International, 90*, 251–258.

Ronkart, S., Blecker, C., Fougnies, C., Van Herck, J. C., Wouters, J., & Paquot, M. (2006). Determination of physical changes of inulin related to sorption isotherms: An X-ray diffraction, modulated differential scanning calorimetry and environmental scanning electron microscopy study. *Carbohydrate Polymers, 63*, 210–217.

Ronkart, S. N., Paquot, M., Blecker, C. S., Fougnies, C., Doran, L., Lambrechts, J. C., ... Deroanne, C. (2009). Impact of the crystallinity on the physical properties of inulin during water sorption. *Food Biophysics, 4*, 49–58.

Ronkart, S. N., Deroanne, C., Paquot, M., Fougnies, C., & Blecker, C. S. (2010). Impact of the crystallisation pathway of inulin on its mono-hydrate to hemi-hydrate thermal transition. *Food Chemistry, 119*, 317–322.

Ronkart, S. N., Paquot, M., Deroanne, C., Fougnies, C., Besbes, S., & Blecker, C. S. (2010). Development of gelling properties of inulin by microfluidization. *Food Hydrocolloids, 24*, 318–324.

Santos, M., Araujo-Andrade, C., Tymczyszyn, E., & Gomez-Zavaglia, A. (2014). Determination of amorphous/rubbery states in freeze-dried prebiotic sugars using a combined approach of near infrared spectroscopy and multivariate analysis. *Food Research International, 64*, 514–519.

Sirbu, A., & Arghire, C. (2017). Functional bread: Effect of inulin-type products addition on dough rheology and bread quality. *Journal of Cereal Science, 75*, 220–227.

Tighe-Neira, R., Alberdi, M., Arce-Johnson, P., Romero-Romero, J. L., Reyes-Díaz, M., & Inostroza-Blancheteau, C. (2017). Foods with functional properties and their potential uses in human health. In N. Shiomi, & V. Waisundara (Eds.). *Superfood and Functional Food-An Overview of Their Processing and Utilization (chapter 9)*. Rijeka, Croatia: InTech.

Tymczyszyn, E. E., Sosa, N., Gerbino, E., Hugo, A., Gómez-Zavaglia, A., & Schebor, C. (2012). Effect of physical properties on the stability of lactobacillus bulgaricus in a freeze-dried galacto-oligosaccharides matrix. *International Journal of Food Microbiology, 155*, 217–221.

Wada, T., Sugatani, J., Terada, E., Ohguchi, M., & Miwa, M. (2005). Physicochemical characterization and biological effects of inulin enzymatically synthesized from sucrose. *Journal of Agricultural and Food Chemistry, 53*, 1246–1253.

Wolkers, W. F., Oliver, A. E., Tablin, F., & Crowe, J. H. (2004). A Fourier-transform infrared spectroscopy study of sugar glasses. *Carbohydrate Research, 339*, 1077–1085.

Zimeri, J. E., & Kokini, J. L. (2002). The effect of moisture content on the crystallinity and glass transition temperature of inulin. *Carbohydrate Polymers, 48*, 299–304.